HOKKAIDO UNIVERSITY

Title	Tough Hydrogels with Fast, Strong, and Reversible Underwater Adhesion Based on a Multiscale Design
Author(s)	Rao, Ping; Sun, Tao Lin; Chen, Liang; Takahashi, Riku; Shinohara, Gento; Guo, Hui; King, Daniel R.; Kurokawa, Takayuki; Gong, Jian Ping
Citation	Advanced Materials, 30(32), 1801884 https://doi.org/10.1002/adma.201801884
Issue Date	2018-08-09
Doc URL	http://hdl.handle.net/2115/75191
Rights	This is the peer reviewed version of the following article: Ping Rao, Tao Lin Sun, Liang Chen, Riku Takahashi, Gento Shinohara, Hui Guo, Daniel R. King, Takayuki Kurokawa, Jian Ping Gong, Tough Hydrogels with Fast, Strong, and Reversible Underwater Adhesion Based on a Multiscale Design, Advanced materials, 2018, 30, 1801884, which has been published in final form at https://doi.org/10.1002/adma.201801884. This article may be used for non-commercial purposes in accordance with Wiley Terms and Conditions for Use of Self-Archived Versions.
Type	article (author version)
Additional Information	There are other files related to this item in HUSCAP. Check the above URL.
File Information	Manuscript(adma201801884).pdf

Tough hydrogels with fast, strong, and reversible underwater adhesion based on a multi-scale design

Ping Rao[1], Tao Lin Sun[2,3,4], Liang Chen[1], Riku Takahashi[1], Gento Shinohara[5], Hui Guo[2], Daniel R. King[2,3], Takayuki Kurokawa[2,3], and Jian Ping Gong[2,3]*

P. Rao, L. Chen, R. Takahashi,

[1]Graduate School of Life Science, Hokkaido University, Sapporo 001-0021, Japan.

Dr. T. L. Sun, Dr. H. Guo, Dr. D. R. King, Prof. T. Kurokawa, Prof. J. P. Gong,
[2]Faculty of Advanced Life Science, Hokkaido University, Sapporo 001-0021, Japan.

Dr. T. L. Sun, Dr. D. R. King, Prof. T. Kurokawa, Prof. J. P. Gong,

[3]Global Institution for Collaborative Research and Education (GI-CoRE), Hokkaido University, Sapporo 001-0021, Japan.

Dr. T. L. Sun,

[4]South China Advanced Institute for Soft Matter Science and Technology, South China University of Technology, Guangzhou 510640, China.

G. Shinohara,

[5]Department of Zoology, National Museum of Nature and Science, Tsukuba 305-0005, Japan.

Prof. J. P. Gong

* Corresponding Author, Email: gong@sci.hokudai.ac.jp

Hydrogels have promising applications in diverse areas, especially wet environments including tissue engineering, wound dressing, bio-medical devices, and underwater soft robotics. Despite strong demands in such applications and great progresses in irreversible bonding of robust hydrogels to diverse synthetic and biological surfaces, tough hydrogels with fast, strong, and reversible underwater adhesion are still not available yet. Herein, we propose a strategy to develop hydrogels demonstrating such characteristics by combining macro-scale surface engineering and nano-scale dynamic bonds. Based on this strategy, we obtained excellent underwater adhesion performance of tough hydrogels with dynamic ionic and hydrogen bonds, on diverse substrates, including hard glasses, soft hydrogels, and biological tissues. The proposed strategy can be generalized to develop other soft materials with underwater adhesion.

Main

Recent progress on the development of various hydrogels with high robustness, large deformation capacity, and diverse functions indicates the great promise of this class of materials for various applications.[1-11] Due to their water-containing nature, the major potential applications of hydrogels are in wet environments, such as artificial organs, tissue engineering, bio-medical devices in the human body, and underwater soft robotics. In many such applications, permanent bonding or reversible attachment of hydrogels to other surfaces, synthetic or natural, hard or soft, is required. However, hydrogels usually show poor adhesion to other surfaces in their fully swollen state. Recently, prominent progress has been achieved

2

on the irreversible robust bonding of hydrogels to diverse synthetic and biological surfaces, which shows that chemical bonding or physical interlocking of the interface and bulk energy dissipation are critical for the robust bonding of the hydrogels.[12-19] On the other hand, the research for in situ underwater adhesion of hydrogels is still at its born.[20-22] The state-of-the-art technology suffers from shortcomings including long contact forming time and very weak adhesion strength. A general strategy to develop hydrogels with fast, strong, and reversible adhesion underwater, is still lacking.

Realization of fast, strong and reversible underwater adhesion of soft materials needs to solve multi-scale and multi-factor problems, involving fluid mechanics, soft matter mechanics, material science, and surface chemistry.[23-25] At the macroscale, the water drainage between two approaching surfaces should be considered. Depending on the contact area and normal pressure, it may take a very long time to squeeze out the interface water during the contact process.[26,27] At the inter-mediate scale, the permanent water entrapment usually occurs at the soft interface. The stronger the adhesion and the softer the gel, the easier it is for water to become trapped. This not only reduces the true contact area, but also acts as a flaw for initiating the debonding at the interface.[28,29] At the nanoscale, the hydrogels usually favour, thermodynamically, the formation of a water film at the interface owing to the strong hydrating ability of hydrophilic polymer strands, which prevents the formation of molecular bridges at the interface.[30]

Here, we present a design strategy to obtain hydrogels with fast, strong, and reversible adhesion underwater by combining energy dissipative hydrogels with dynamic bonds and bio-inspired surface drainage architecture. First, we choose hydrogels with dynamic bonds for their high capacity of energy dissipation that favours toughness and strong adhesion. Most importantly, they are intrinsically adhesive in water. Since dynamic bonds are reversible in

3

swollen hydrogels and contribute to the toughness and self-recovery of the hydrogels, they also have the potential to form reversible bridges with other surfaces in wet environments when properly choosing the surface chemistry of the substrates. In this study, we first select a charge-balanced polyampholyte (PA) hydrogel[31-33] with dynamic ionic bonds and then a tough and self-recovery hydrogel with dynamic hydrogen bonds. The PA hydrogels are generated by using the random copolymerization of the sodium p-styrenesulfonate (NaSS) anionic monomer, and the methyl chloride quarternized *N,N*-dimethylamino ethylacrylate (DMAEA-Q) cationic monomer, with a very small amount of chemical cross-linker (Figure S1, Supplementary Information). Given the dynamic nature of the ionic bonds, the PA gel is strongly viscoelastic (Figure S2, Supplementary Information), and it exhibits superior strength and toughness (Figure S3a, Supplementary Information). Moreover, as revealed by the Mooney-Rivlin plot,[34] it shows strain softening and then strain-hardening (Figure S3b, Supplementary Information). The gel also shows excellent self-recovery and the time for the full self-recovery increases with the applied strain (Figure S4, Supplementary Information). The ionic bonds exchanging time is in the ms range.[32] These results suggest that this PA gel is a suitable candidate as an underwater adhesive.

Then, in order to obtain fast water drainage at the gel-substrate interface, we analyzed the clingfish that shows fast and reversible adhesion to various surfaces underwater. The adhesive disc of the clingfish has many hexagonal features separated by interconnecting grooves (**Figure 1**a) that are considered to enhance the water drainage rate.[35-36] Inspired by the clingfish, we engineered the gel surface with hexagonal facets separated by interconnecting grooves (Figure 1b). Such interconnecting surface grooves serve as channels for fast water drainage during contact underwater (Figure 1c). Once the hexagonal facets are in contact with the substrate, the dynamic bonds of the hydrogel form bridges with the

substrate (Figure 1d). In addition to the good contact formation, the discontinuous hexagonal facets also have effects on increasing the compliance of the gel and on preventing continuous crack propagation throughout the interface, similar to the contact splitting effect observed for micro-fibrillar surfaces.[37-40] These two effects significantly enhance the bulk gel energy dissipation[12,19,23] and delay the interfacial debonding (Figure 1e), leading to strong yet reversible adhesion.

To avoid water-drop trapping at the interface, we need to design hexagonal facets with proper sizes (Figure 1f). Since the water-drop trapping is governed by the competition between the elastic energy to deform the gel and the adhesive energy of the gel to the substrate, the size of the hexagonal facets should not be much larger than the elastic length, l_0, that is determined by equation: $l_0 = W/G'$, where W and G' are the adhesion energy per unit area of the gel to the substrate and the storage shear modulus of the gel, respectively.[41] The adhesion energy for the adhesion of a PA gel onto a glass substrate in air is ~50 J/m^2.[42] Using the storage shear modulus G' of the PA gel as ~30 kPa at the low frequency limit (Figure S2, Supplementary Information), the elastic length of the PA-glass system is approximately 1 mm. Using silicone molds (Figure S5, Supplementary Information), we subsequently prepared two sets of gels having hexagonal facets of 0.875 mm (sample P1) and 1.75 mm (sample P2) in length (***a***). The height of hexagonal facets (***h***), groove width (***w***), and total thickness (***h+t***) were kept the same as 0.483, 0.656, and 2.19 mm, respectively, for the two samples. A control sample that does not contain hexagonal facets with the same total thickness was also prepared, labelled as sample P0 (see "Experimental Section" and Table S1, Supplementary Information). **Figure 2**a shows the typical optical and microscopic images of the surface engineered PA gel (P1). Well-defined hexagonal facets separated by grooves are formed on the gel surface.

To test the idea, we first observed the evolution of the contact formation underwater

for flat and surface engineered PA gels using a home-made set-up using critical refraction,[29] as shown in Figure 2b. In brief, a gel disc with diameter of 35 mm and total thickness of 2.19 mm was placed on the upper side of the substrate with the engineered surface. A trapezoidal prism, attached to the load cell, approached the gel in water from above, at a steady rate of 10 μm/s until the normal force reached the 15 N designed value, and then was held in that position (Figure 2c-i, and c-ii). The corresponding nominal pressure estimated from the projected area of the sample surface was 15.6 kPa. During this process, the contact image of the gel to the prism surface was observed from an angle between the critical refraction angles of water θ_w and the gel θ_g (Figure 2b).

Figure 2d shows snapshots of the contact images, where the bright region is in contact with the glass and the dark region is trapped with water, for the three samples: P0, P1, and P2. For the flat PA gel (P0), the contact started from the periphery then gradually and irregularly developed into the whole region as time elapsed. The normal force rapidly reached the pre-set value after 22 s (Figure 2c-ii), although the gel was hardly in contact with the substrate yet, indicating that the interface is intermediated by water. Even after more than 1000 s, some regions still remained dark, with lots of dark points distributed heterogeneously, indicating the permanent entrapment of water (see Movie S1, Supplementary Information). It should be mentioned that the compressive strain rate applied to the sample, estimated from the contact rate and sample thickness, was about 4×10^{-3} s^{-1} ($\sim2.5\times10^{-2}$ rad/s). At this strain rate, the PA sample was very soft (storage shear modulus of ~30 kPa, as shown in Figure S2, Supplementary Information), and the 15.6 kPa nominal pressure gave a compressive deformation of ~50% average to the flat gel, which is large enough to cause full contact if there is no water entrapment.

On the other hand, the contacting process finished within 30–40 s for both the P1 and

6

P2 samples, much faster than the flat sample that took more than 1000 s. For the P2 sample, the center of each hexagonal facet remained dark even after more than 1000 s, suggesting that the water trapping occurred for this hexagonal facet size, while, for the P1 sample, each hexagonal facet became brighter, indicating that the water drop trapping is completely suppressed for this facet size. These results imply that the critical length for the water trapping to occur is between 0.875 and 1.75 mm for this PA gel-glass system at the relevant strain rate, which is consistent with the estimated scale for the elastic length.

From the time profile of the contact area formation, we observed that the surface engineered samples form contacts with the substrate much quicker than the flat sample. The P1 sample forms full contact while the P2 sample forms 85.8% contact relative to the hexagonal facet area at equilibrium due to water entrapment (Figure 2c-iii), however the time to reach the equilibrium contact area is almost identical for these two samples within the time resolution of the experiment. The above results indicate that engineering the hydrogel surfaces with millimeter-scale facets leads to quick underwater contact.

Further, we observed that the quick contact of the surface engineered gels induced quick and strong adhesion to the rigid glass using only light compression, while the flat PA gel did not (Movie S2, Supplementary Information). The surface engineered PA gels also showed good adhesion to soft surfaces including the flat PA gel (Movie S3, Supplementary Information) and tissue (Movie S4, Supplementary Information). For the first case, we cut one piece of P1 sample into two pieces and tested the self-adhesion between different surfaces underwater. The engineered surface strongly adhered to the flat surface, while the self-adhesion of flat-on-flat and engineered-on-engineered surfaces was very weak. The poor adhesion between flat surfaces is apparently due to the long water drainage time at the interface while the poor adhesion between the engineered surfaces should be attributed to the

decreased contact area even though water drainage was fast.

To measure the adhesion strength, we used the standard probe tack test[41] with a set-up as illustrated in Figure S6, Supplementary Information. In brief, the PA gel (15 mm diameter) was compressed onto the glass substrate underwater at a steady contact rate of 10 μm/s until the contact force increased to 1 N, corresponding to a 5.7 kPa nominal pressure. Then, the gel was held in that position for 10 s, and finally, it was retracted from the substrate at a steady debonding rate of 10 μm/s (see the Experimental Section for details).

The displacement-time and force-time profiles of the three samples on glass are shown in **Figure 3**a. The glass we used was first washed by acetone and then washed by deionized water. It carried negative surface charges, and the Zeta potential measured in 10 mM sodium chloride (NaCl) aqueous solution was -32.44 mV and the contact angle to water was $19.6 \pm 2.2°$ at the temperature of 25 °C. The surface engineered PA gels showed much stronger debonding forces and larger deformation than the flat PA gel. Furthermore, the P1 sample showed stronger adhesion than the P2 sample, as seen from both the maximum force and the deformation at the maximum debonding force. It should be mentioned that even considering partial contact of P2 due to the entrapment of water drops, the true contact area of P2 was larger than that of P1.

From these results, we concluded that the poor contact of the P0 sample is due to the slow water drainage, while the entrapment of water drops leads to the poor contact of P2 relative to P1. In addition to such effect of the contact area, crack initiation and propagation at the interface also play important roles in underwater adhesion. The energy needed to initiate the crack is generally much higher than that of crack propagation. For the flat gel, there are more trapped water areas acting as flaws, making it much easier to initiate and propagate the crack. However, for the surface engineered hydrogel, less flaws exist and the pillars are

independent from one other. To overcome all the bonded pillars, frequently crack re-initiation is needed, which largely delayed the debonding of the adhesive. This is confirmed by observing the interface during debonding (Figure 3b and Movie S5, Supplementary Information). Furthermore, the difference in the deformability of the samples during detachment should also play an important role in the adhesion, strength, and debonding energy per unit area, as suggested by the change in the deformation of these samples. As shown in Figure 3a, the debonding of the P1 sample was largely delayed compared to P2 and P0. This indicates that the P1 sample was substantially stretched during the debonding process, and clearly illustrates the effect of bulk energy dissipation on adhesion strength and debonding energy per unit area during the detachment process.

Since the rigid glass substrate does not contribute to the debonding energy dissipation, we proceeded to study the adhesion of the patterned gels on soft and energy dissipative substrates using the flat PA gel as a counter substrate. The results are shown in Figure 3c. The trend of adhesion strength is identical to that of the glass substrate, that is, the P1 sample showed higher adhesion strength than the P2 sample, and the flat sample showed the weakest adhesion of all three samples. However, comparing these results with those for the flat glass substrate, both the maximum debonding force and the deformation on the soft PA gel are systematically higher. These results suggest that the contact formation process on the flat PA gel is similar to that on glass, while the interfacial bridging strength and bulk deformability of the soft substrate are much larger than the rigid glass substrate, which substantially delays the debonding. Observation of the interface during the tack test (Figure 3d and Movie S6, Supplementary Information) showed that for the flat gel, only a small part of the interface was in contact with the soft substrate while for the P1 sample, most of the hexagonal facets were in good contact with the substrate. We also confirmed that the soft substrate was substantially

deformed during the debonding process. Furthermore, the delayed fracture due to the independent crack propagation and the increased compliance of the system was also confirmed in the debonding process of the engineered surface. The P1 gel in particular, was significantly stretched during detachment.

Given the reversible nature of the ionic bonds, the adhesion of the PA hydrogels is, in principal, reversible. Furthermore, we quantitatively investigated the adhesion reversibility for the surface engineered PA gels on flat PA gels by conducting cyclic tack tests at different waiting times while maintaining the other conditions as described above. As shown in Figure 3e and f, for the P2 sample, the probe tack test curves with different waiting times from 1 to 30 min almost overlapped, and ~ 90% of the adhesion strength and debonding work were recovered within 1 min. These results indicate excellent reversibility. On the other hand, the P1 sample, with higher maximum debonding force and larger debonding deformation than the P2 sample, only showed partial recovery even after 30 min waiting, and the adhesion force and energy decreased with the cyclic test. This result suggests that it took longer for the P1 sample to recover, due to the significant stretching during debonding. During this process, significant number of primary bonds in the bulk gel are broken. These broken bonds form temporary bonds with other ionic groups during the recovery process, resulting in much longer recovery times. This is confirmed by the underwater cyclic tensile behaviors of the PA gel at different maximum strains (Figure S4, Supplementary Information). The hysteresis area between the loading and unloading curves, corresponding to the amount of broken bonds during loading, increases with the maximum strain. The recovery ratio of the hysteresis at different waiting times, corresponding to the reforming of the ionic bonds between the original ion pairs, increases with the waiting time between subsequent cycles.[31] At a relatively small strain, $\varepsilon=3$, the sample fully recovered within 1 min, while it took 15 min for

10

the full recovery when $\varepsilon=6$. At a larger strain, $\varepsilon=8$, the sample did not show full recovery even after 45 min. From the debonding deformation, the maximum tensile strain at the debonding point was determined as 3.5 for the P2 sample and 10.0 for the P1 sample. The large difference in the maximum tensile strain values accounts for the reversibility differences between the P2 and P1 samples, therefore, it is a compromise between high adhesion strength and fast reversibility. For a hydrogel with given mechanical properties and self-recovery kinetics, we need to design proper size hexagonal facets to balance the strong underwater adhesion and reversibility for a given waiting time.

We also conducted underwater probe tack tests (maintaining the conditions mentioned above) on diverse substrates varying from hard to soft, including copper plate, polystyrene (PS), and pork heart tissue. The adhesion strength, calculated from the ratio of the debonding peak force to the surface area of the PA gel, and the debonding energy per unit area, calculated from the area under the force-displacement curve and the surface area of the PA gel, are summarized in **Figure 4**a and b, respectively. It should be emphasized that the adhesion strength and debonding work are as high as ~25 kPa and ~50 J/m^2, respectively, for the P1 sample on the flat PA gel. This adhesion strength is as high as 1/3 of the gecko that shows strong adhesion in air.[41] Considering that the adhesion tests were performed under a very weak compressive pressure (5.7 kPa, or 60 g/cm^2) for a very short contact time (10 s), the results in Figure 4 indicate a significant progress in comparing with previously reported underwater adhesion of bulk hydrogels that lack water-drainage mechanism and energy dissipation mechanism.[21, 22]

The strategy of combining macroscale surface engineering and micro-scale dynamic bonds is applicable to various recently developed tough hydrogels based on hydrogen and ionic bonds, hydrophobic interaction, coordinate bonds, etc.[16,31,32,44,45,46] For example, a

surface engineered tough hydrogel based on hydrogen bonding, synthesized from copolymerization of poly(ethylene glycol)$_{200}$ monomethyl ether monomethacrylate ((PEG)$_{200}$OMe) macromer and acrylic acid monomer (denoted as POA hydrogel), shows similar trends of underwater adhesion behavior on glass and tissue as PA gels, as shown in Figure 4 (for more details see Figure S7, Supplementary Information).

In summary, the above success in developing hydrogels showing fast, strong, and reversible underwater adhesion is due to the synergetic effect brought about by integrating macroscopic surface engineering and the tough hydrogels with dynamic bonds. The surface grooves not only accelerate water drainage and prevent water trapping, but also delay crack propagation during detachment. Specifically, the discontinuous contact pattern leads to independent detachment of contacts, which requires re-initiation of the crack for each contact. The splitting of contact also leads to an increase in the compliance of the contact point, which significantly enhances the bulk deformation of the gel. The dynamic bonds of the gel not only form reversible bridges at the interface to show reversible adhesion, but also dissipate a significant amount of energy in bulk during deformation. Smaller feature sizes lead to stronger underwater adhesion but poorer reversibility as the self-recovery time increases with the deformation at debonding. Such trade-off relations, determined by the adhesion strength, the modulus, and the self-recovery kinetics of the hydrogel, should be considered when designing the size of the surface features. This research could be used in some hydrogels applications requiring fast and reversible adhesion in wet environments or underwater, such as re-usable sheets for wound dressing, temporary adhesives for tissue healing, and anti-slippery gloves for wall-climbing robotics. The proposed method is simple but effective, and suitable for large-scale manufacturing with feature size dimensions of several millimeters.

Experimental Section

Synthesis of PA patterned hydrogels: Polyampholyte hydrogels were prepared by the random copolymerization of the sodium p-styrenesulfonate (NaSS) anionic monomer and the methyl chloride quarternized *N,N*-dimethylamino ethylacrylate (DMAEA-Q) cationic monomer at a monomer ratio of 0.52 : 0.48, as described in previous studies.[33] An aqueous solution containing 2.5 M total monomer concentration, 2.5 mM, 2-oxoglutaric acid as UV initiator, and 2.5 mM N,N-methylenebisacrylamide crosslinker was poured into a reaction cell, then irradiated with 365 nm UV light for 10 h. After polymerization, the gel was immersed in excess amount of water for 1 week to dialyze the mobile counter-ions, and allow the oppositely charged polyions on the copolymers to form stable ionic complexes through intra- or inter-chain interactions. The PA gel deswelled to 87.5% of its as-prepared size in each direction after dialysis, and became very tough. To induce surface groove features, the gelation of the PA gels was performed in a rectangular reaction cell with a 2.0 mm thick spacer where one cell wall was made from a silicone mold with honeycomb-like grid structure (Figure S5). The width (*w'*) and height (*h'*) of the grid molds were kept constant at 0.75, and 0.5 mm, respectively, while the hexagon side length (a') of the ridge varied from 1 to 2 mm. The size of the grooves on the PA gel surface was tailored using the grid of the mold and the total thickness of the gel using the silicone spacer, but all these sizes were reduced to 87.5% due to the deswelling of the gel by dialysis.

Synthesis of POA patterned hydrogels: The tough P((PEG)$_{200}$OMe-co-AAc) (denoted as POA) hydrogels with hydrogen bonds were prepared using the random copolymerization of the poly(ethylene glycol)$_{200}$ monomethyl ether monomethacrylate ((PEG)$_{200}$OMe) macromer, and acrylic acid (AAc) monomer with a 1.5 molar ratio of PEG segments in (PEG)$_{200}$OMe to pendant carboxylic acids in AAc. The POA hydrogels were prepared using the similar

13

procedure as the polyampholyte (PA) hydrogels from a dimethyl sulfoxide (DMSO) solution containing 2 M in total macromer and monomer, and 2 mM 2-oxoglutaric acid as UV initiator. After the gelation, the POA hydrogels were immersed in water to remove the DMSO and allow the forming of hydrogen bonds. The POA hydrogels deswelled to 81% of their as-prepared size in each direction in water.

In situ observation of the underwater contact formation evolution: A 35 mm diameter disc shaped gel (flat or patterned) was placed on a plastic substrate in the stage box filled with water. An isosceles trapezoidal prism (angle 70°, length 66 mm, height 22.08 mm, and width 50 mm), attached to the load cell using a rigid holder, approached the gel from the top at a steady 10 μm/s rate until the force reached the designed 15 N value. At the same time, the contact image of the gel on the prism surface was observed from an angle between the critical angles of water and gel using a zoom camera. The evolution of the contact image in time was subsequently recorded at the fixed displacement for different samples (see Movie S1, Supplementary Information). The contact areas for these snapshots at different times were calculated using the Image-J software, and the contact area ratios were calculated respective to the nominal area of the flat sample or the hexagonal pads area of the patterned gels.

Underwater probe tack test. The probe tack tests, for measuring the adhesion strength and energy dissipation of the hydrogels, were performed on a Shimadzu Autograph AG-X 20 kN tensile machine in water at 25 °C. The set-up consisted of mainly two parts (Figure 6, Supplementary Information): the bottom part, a cell with a rigid stage providing the deionized water environment for the tack test, and the upper one, a copper shaft connected with the load cell. The gel was cut into disc shapes of prescribed diameter, and bonded to the copper shaft using a very thin super glue film (Konishi Co. Ltd.). Copper plate, glass plate, polystyrene plate, flat PA gel, and pork heart tissue, are used as counter substrates. The glass used was

micro slide glass made by the MATSUNAMI Company of Japan (product number S2112). The glass was first washed by acetone and then washed by deionized water. The glass carried negative surface charges, and the Zeta potential measured in 10 mM sodium chloride (NaCl) aqueous solution was - 32.44 mV, measured by the Zeta potential and Particle size analyzer (ELSZ-2000, Otsuka Electronics Co., Ltd (Osaka, Japan)). The contact angle to water was $19.6 \pm 2.2°$ at 25 °C. Fresh pork heart and beef heart was purchased from Nippon Food Packer Inc. (Japan) and used as received without any surface pretreatment. Before beginning measurements, the whole system was immersed in water and waited for 30 min for the equilibrium state to be reached.

For the test, the upper gel was first compressed to the lower substrate at a constant compressing rate of 10 µm/s until it reached the set force 1 N. Afterward, the sample was held in this position for the described contact time 10 s. Subsequently, the probe was retracted at a constant rate of 10 µm/s until the debonding finished. The force, displacement, and time were recorded during the process.

Other experimental details are shown in Supplementary Information.

Supplementary Information

Supplementary Information is available from the Wiley Online Library or from the author.

data of the glass plate.

Conflict of Interest

The authors declare no conflict of interest.

References

[1]   J. P. Gong, Y. Katsuyama, T. Kurokawa, Y. Osada, *Adv. Mater.* **2003**, *15*, 1155.

[2]   J. -Y. Sun, X. Zhao, W. R. K. Illeperuma, O. Chaudhuri, K. H. Oh, D. J. Mooney, J. J. Vlassak, Z. Suo, *Nature* **2012**, *489*, 133.

[3]   H. J. Zhang, T. L. Sun, A. K. Zhang, Y. Ikura, T. Nakajima, T. Nonoyama, T. Kurokawa, Y. Katsuyama, T. Kurokawa, O. Ito, H. Ishitobi, J. P. Gong, *Adv. Mater.* **2016**, *28*, 4884.

[4]   D. R. King, T. L. Sun, Y. Huang, T. Kurokawa, T. Nonoyama, A. J. Crosby, J. P. Gong, *Mater. Horiz.* **2015**, *2*, 584.

[5]   S. Naficy, H. R. Brown, J. M. Razal, G. M. Spinks, P. G. Whitten, *Aust. J. Chem.* **2011**, *64*, 1007.

[6]   D. J. Beebe, J. S. Moore, J. M. Bauer, Q. Yu, R. H. Liu, C. Devadoss, B. –H. Jo, *Nature* **2000**, *404*, 588.

[7]   A. Richter, G. Paschew, S. Klatt, J. Lienig, K. –F. Arndt, H. -J. P. Adler, *Sensors* **2008**, *8*, 561.

[8]   M. A. Haque, G. Kamita, T. Kurokawa, K. Tsujii, J. P. Gong, *Adv. Mater.* **2010**, *22*, 5110.

[9]   T. Miyata, N. Asami, T. Uragami, *Nature* **1999**, *399*, 766.

[10]   E. Ruel-Gariepy, J. C. Leroux, *Eur. J. Pharm. Biopharm.* **2004**, *58*, 409.

[11]   G. W. Ashley, J. Henise, R. Reid, D. V. Santi, *Proc. Natl. Acad. Sci. U.S.A.* **2013**, *110*, 2318.

[12]   T. Kurokawa, H. Furukawa, W. Wang, Y. Tanaka, J. P. Gong, *Acta Biomater.* **2010**, *6*, 1353.

[13]   D. L. Hern, J. A. Hubbell, *J. Biomed. Mater. Res.* **1998**, *32*, 266.

[14]   S. Y. Yang, E. D. O'Cearbhaill, K. M. Park, W. K. Cho, M. Villiger, B. E. Bouma, B. Pomahac, J. M. Karp, *Nat. Commun.* **2013**, *4*, 1702.

[15]   C. J. Wu, J. J. Wilker, G. Schmidt, *Macromol. Biosci.* **2013**, *13*, 59.

[16]   M. Nakahata, Y. Takashima, H. Yamaguchi, A. Harada, *Nat. Commun.* **2011**, *2*, 511.

[17]   M. T. I. Mredha, N. Kitamura, T. Nonoyama, S. Wada, K. Goto, X. Zhang, T. Nakajima, T. Kurokawa, Y. Takagi, K. Yasuda, J. P. Gong. *Biomaterials* **2017**, *132*, 85.

[18]   T. Nonoyama, S. Wada, R. Kiyama, N. Kitamura, M. T. I. Mredha, X. Zhang, T. Kurokawa, T. Nakajima, Y. Takagi, K. Yasusa, J. P. Gong, *Adv. Mater.* **2016**, *28*, 6740.

[19]   H. Yuk, T. Zhang, S. Lin, G. A. Parada, X. Zhao, *Nat. Mater.* **2016**, *15*, 190.

[20]   S. Rose, A. Prevoteau, P. Elzière, D. Hourdet, A. Marcellan, L. Leibler, *Nature* **2014**, *505*, 382.

[21]   L. C. Bradley, N. D. Bade, L. M. Mariani, K. T. Turner. *ACS Appl. Mater. Interfaces* **2017**, *9*, 27409.

[22]   G. Sudre, L. Olanier, Y. Tran, D. Hourdet, C. Creton, *Soft Matter* **2012**, *8*, 8184.

[23]   J. Li, A. D. Celiz, J. Yang, Q. Yang, I. Wamala, W. Whyte, B. R. Seo, N. V. Vasilyev, J. J. Vlassak, Z. Suo, D. J. Mooney, *Science* **2017**, *357*, 378.

[24]   L. Khandeparker, A. C. Anil, *Int. J. Adhes. Adhes.* **2007,** *27*, 165.

[25]   Z. Qin, M. J. Buehler, *J. Mech. Phys. S.* **2014**, *62*, 19.

[26]   R. Gupta, J. Frechette, *Langmuir* **2012**, *28*, 14703.

[27]   J. H. Waite, *Chemtech* **1987**, *17*, 692.

[28]   J. Ahmed, H. Guo, T. Yamamoto, T. Kurokawa, M. Takahata, T. Nakajima, J. P. Gong, *Macromolecules* **2014**, *47*, 3101.

[29]   T. Yamamoto, T. Kurokawa, J. Ahmed, G. Kamita, S. Yashima, Y. Furukawa, Y. Ota, H. Furukawa, J. P. Gong, *Soft Matter* **2014**, *10*, 5589-5596.

[30]   D. J. Broesch, J. Frechette, *Langmuir* **2012**, *28*, 15548.

[31]   T. L. Sun, T. Kurokawa, S. Kuroda, A. B. Ihsan, T. Akasaki, K. Sato, M. A. Haque, T. Nakajima, J. P. Gong, *Nat. Mater.* **2013**, *12*, 932.

[32]   A. B. Ihsan, T. L. Sun, T. Kurokawa, S. N. Karobi, T. Nakajima, T. Nonoyama, C. K. Roy, F. Luo, J. P. Gong, *Macromolecules* **2016**, *49*, 4245.

[33]   T. L. Sun, F. Luo, T. Kurokawa, S. N. Karobi, T. Nakajima, J. P. Gong, *Soft Matter* **2015**, *11*, 9355.

[34]   R. E. Webber, C. Creton, H. R. Brown, J. P. Gong, *Macromolecules* **2007**, *40*, 2919.

[35]   D. K. Wainwright, T. Kleinteich, A. Kleinteich, S. N. Gorb, A. P. Summers, *Biol. Lett.* **2013**, *9*, 20130234.

[36]   P. Ditsche, D. K. Wainwright, A. P. Summers, *J. Exp. Biol.* **2014**, *217*, 2548.

[37]   E. Arzt, S. Gorb, R. Spolenak, *Proc. Natl. Acad. Sci. U.S.A.* **2003**, *100*, 10603.

[38]   R. Spolenak, S. Gorb, E. Arzt, *Acta Biomater.* **2005**, *1*, 5.

[39]   M. Kamperman, E. Kroner, A. del Campo, R. M. McMeeking, E. Arzt, *Adv. Eng. Mater.* **2010**, *12*, 335.

[40]   A. del Campo, C. Greiner, E. Arzt, *Langmuir* **2007**, *23*, 10235.

[41]   C. Creton, M. Ciccotti, *Rep. Prog. Phys.* **2016**, *79*, 046601.

[42]   C. K. Roy, H. L. Guo, T. L. Sun, A. B. Ihsan, T. Kurokawa, M. Takahata, T. Nonoyama, T. Nakajima, J. P. Gong, *Adv. Mater.* **2015**, *27*, 7344.

[43]   H. Lee, B. P. Lee, P. B. Messersmith, *Nature* **2007**, *448*, 338.

[44]   D. C. Tuncaboylu, M. Sari, W. Oppermann, O. Okay, *Macromolecules* **2011**, *44*, 4997.

[45]   F. Luo, T. L. Sun, T. Nakajima, T. Kurokawa, Y. Zhao, K. Sato, A. B. Ihsan, X. Li, H. Guo, J. P. Gong, *Adv. Mater.* **2015**, *27*, 2722.

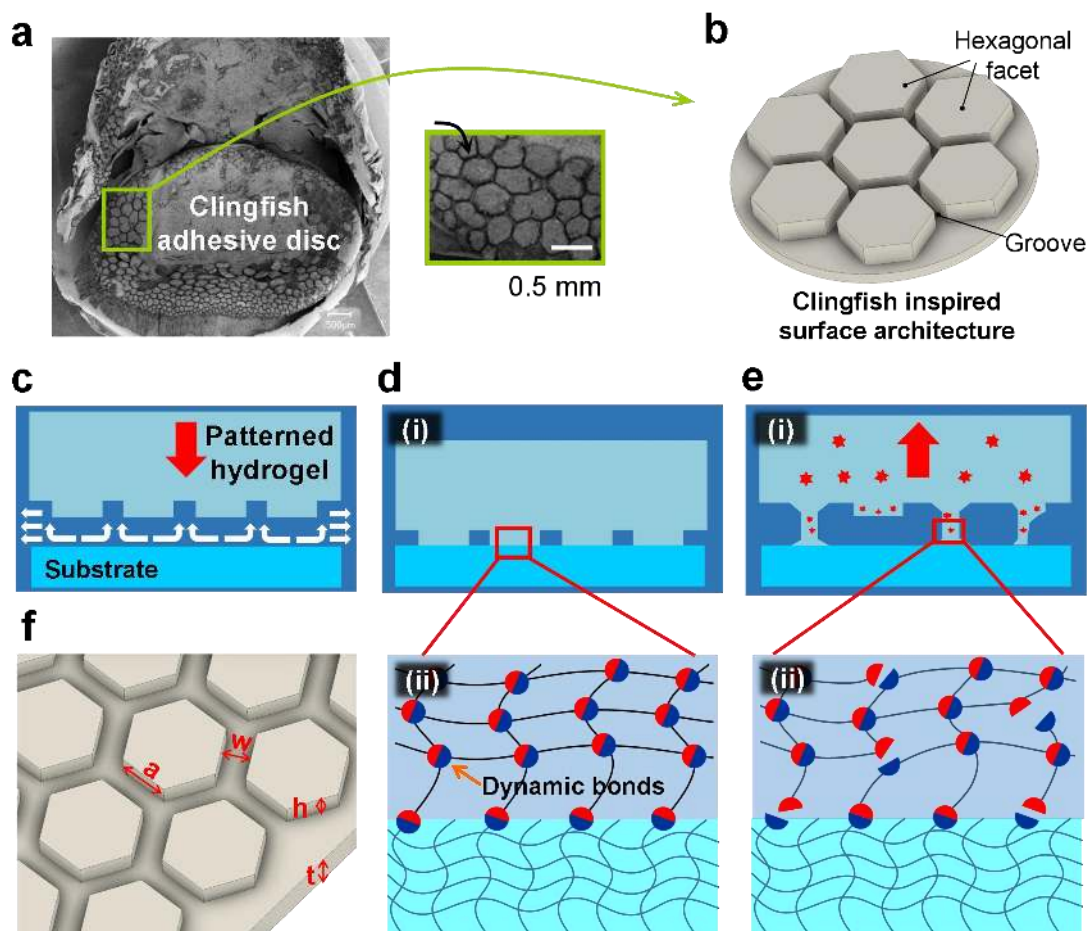[46]   T. Kakuta, Y. Takashima, M. Nakahata, M. Otsubo, H. Yamaguchi, A. Harada. *Adv. Mater.* **2013**, *25*, 2849.

Figure 1. Schematic illustration of the multi-scale design of tough hydrogels with fast, strong, and reversible underwater adhesion. Inspired from the geometry of the adhesive discs of clingfish a). A tough hydrogel with hexagonal facets separated by grooves and dynamic bonds was surface engineered b). The grooves work as water drainage channels to facilitate the fast contact of the hexagonal facets with the substrate underwater c). The dynamic bonds on the hexagonal facets of the gel form bonds with the substrates to bridge the interface d). During stretching, the rupture of bulk dynamic bonds dissipates energy, which delays the debonding at the interface e). Moreover, the independent hexagonal facets prevent continuous crack propagation throughout the interface thus also enhancing the adhesion strength and debonding energy f). The adhesion of the hydrogel is reversible due to reversible dynamic bonding. The dimensions of the surface geometry strongly influence the adhesion behaviour.
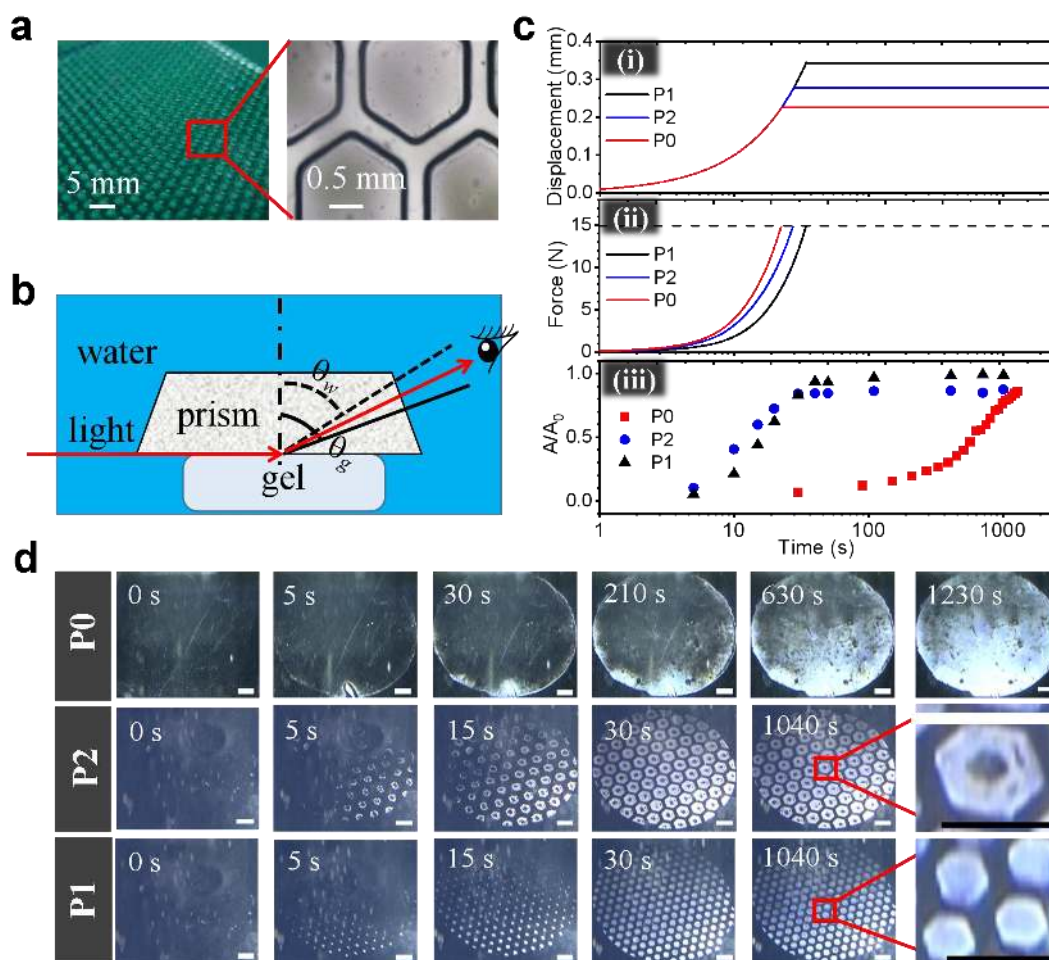
Figure 2. In situ observation of the underwater contact evolution for surface engineered hydrogels on glass substrates. a) Optical and microscopic images of the surface structure of a polyampholyte (PA) hydrogel (sample P2). b) Illustration of the set-up to observe the contact evolution in water. The prism was pushed toward the sample gel at a 10 μm/s rate until the load reached 15 N and then it was held in that position. c) Time profiles of prism displacement (i), normal force (ii), and contact area ratio (A/A_0) (iii) during the contact test. d) Snapshots of the contact images for the P0, P1, and P2 samples. The bright region is in contact with the glass and the dark region is trapped by water. The contact area ratio A was estimated from d) while A_0 is the nominal area of the hexagonal facets. Scale bars: 4 mm.
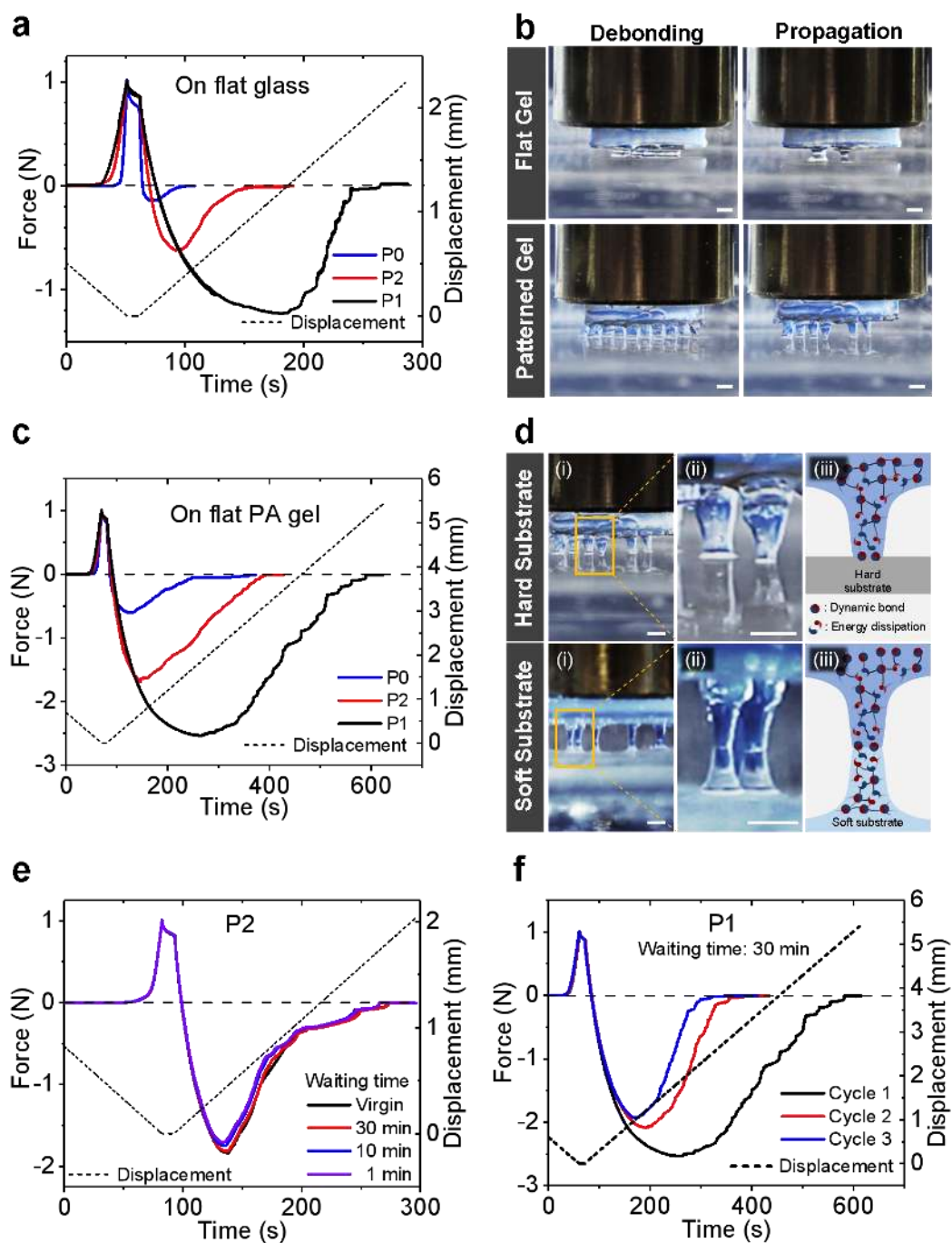
Figure 3. Strong and reversible underwater adhesion of surface engineered PA hydrogels. a) Displacement and force-time profiles of underwater tack tests on a flat glass plate for PA gels with different surface patterns. b) Optical images of the deformation evolution of flat and patterned gels during debonding from the glass plate. c) Displacement and force-time profiles of underwater tack tests on the flat PA gel for PA gels with different surface patterns. d) Optical images of the deformation of the P1 sample on hard glass and soft PA gel. e) Displacement and force - time profiles for cyclic probe tack tests at varied waiting times between successive measurements for a P2 sample on flat PA gel. f) Displacement and force - time profiles for cyclic probe tack tests at 30 min waiting time for a P1 sample on flat PA gel.

P0, P1, and P2 represent the PA gels with flat surface, hexagon facets length (a) of 0.875 and 1.75 mm, respectively. Scale bars: 2 mm.
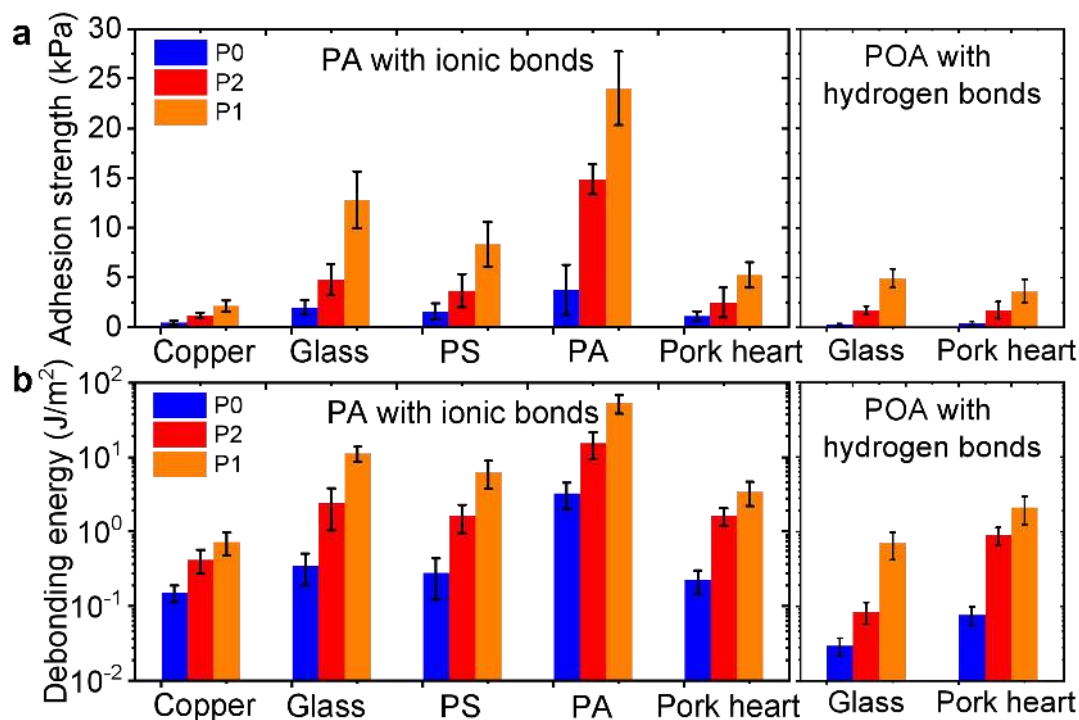

Figure 4. Underwater adhesion strength of surface engineered tough hydrogels with dynamic bonds on diverse substrates. Results for PA hydrogels based on ionic bonds and for POA hydrogels based on hydrogen bonds. a) Adhesion strength, calculated from the ratio of the debonding peak force to the nominal surface area of the samples and b) Debonding energy per unit area, calculated from the ratio of the area under the force-displacement curves to the nominal surface area of the sample. For patterned gels, the facet area was used. Error bars are standard deviation for n=3-5 measurements. Sample diameter 15 mm; contact and debonding rate: 10 µm/s; contact force: 1 N (nominal pressure: 5.7 kPa), holding time: 10 s. PS: polystyrene used for Petri dishes; PA: flat PA gels.